Powder Technology 373 (2020) 336–346

Contents lists available at ScienceDirect

Powder Technology

journal homepage: www.elsevier.com/locate/powtec

Comparative performance of granular scaling laws for lightweight grouser wheels in sand and lunar simulant

Andrew Thoesen, Teresa McBryan, Darwin Mick, Marko Green, Justin Martia, Hamid Marvi *

Arizona State University School for Engineering of Matter, Transport and Energy 501 E Tyler Mall, Tempe, AZ 85287, United States of America

ARTICLE INFO

Article history:
Received 8 April 2020
Received in revised form 17 May 2020
Accepted 30 May 2020
Available online 26 June 2020

Keywords:
Granular matter
Soil mechanics
Granular material
Discrete element method
Lunar simulant
Scaling Laws

ABSTRACT

Recently developed granular scaling laws create new opportunities to evaluate particle dynamics between environment and wheel shapes. We investigate the performance of straight grousered (i.e. protrusions added to the wheel rim to better engage the soil) wheels and helical grousered wheels in both silica sand and crushed basalt lunar simulant. Mechanical power draw and velocity of the wheels are compared in both materials for performance assessment. The scaling laws are evaluated for Earth gravity experimentally and reduced gravity through coupled multi-body dynamic and discrete element method (MBD-DEM) simulations. Experimental results show general power prediction error between 20 and 35% for crushed basalt and 15–25% error for silica sand. Velocity prediction error showed high dependence on material, with silica sand error generally between 4 and 10% and crushed basalt varied between 0 and 27%. Simulation results match theoretical predictions more closely with power error under 8% and velocity error under 4% for most speeds. The experimental error was further investigated and shows a new scaling dependency on sinkage (depth which the wheel rim sinks below the terrain surface) thresholds.

1. Introduction

Granular mechanics as a field tends to favor empirical or semi-empirical approaches. This was the precedent set by Bekker [1,2] including for lunar mobility [3]. Later, Wong [4] made advancements in examining many different soil-geometry models, including those with gravity variation. For example, using weight-offset for rover testing for space applications could have erroneous and at times even opposite results compared to those in parabolic testing [5] due to the gravity compaction of grains. Recent efforts have been assisted by integrated wheel sensors [6] or predictive algorithms [7], but the broadest solutions will be design-independent. In recent years [8], the emergence of more holistic understanding of granular-geometry interaction has occurred. One example is the newly developed granular resistive force theory (RFT), an examination of granular material reactions [9–13] driven by a similar theory used in fluid dynamics. RFT has shown impressive predictive results for certain intruders with a few characterizing tests of the media [11]. This theory has been recently reconciled with the granular physics which assumes the target environment to be a continuum obeying certain characteristics [14,15] that allows for non-dimensional analysis of the movement of wheeled craft in that environment. These Granular Scaling Laws (GSL) recently developed in the literature [15] allow scaling of various wheel parameters such as size and mass to relate certain wheel outputs such as velocity and power for wheels of the same general shape in the same granular media. The advantage of exploiting these non-dimensional parameters is the ability to extrapolate performance of fully-sized vehicles from smaller prototype versions without apriori knowledge of soil characteristics. This could give greater flexibility to mechanical design, experimental environment, and types of vehicle dynamics that can be explored. These laws include a gravity variant version which implies potential for furthering development of space vehicle dynamics as well.

In this study, we explore the effect of both environmental media and wheel shape on these scaling laws. We provide insights and recommendations for wheel testing and how the granular mechanics of wheel-media interface are affected. We evaluate a circular wheel with straight grousers (seen in Fig. 1), and a circular wheel with helical grousers we refer to as “bihelix”. The power and velocity characteristics of these are analyzed and the predictive performance of recently developed granular scaling laws (GSL) in the literature [15] are applied, for the first time, to several areas:

1. Evaluation in a lunar regolith analogue, BP-1 [25], a weakly cohesive, highly angular and interlocked media. Identical tests are performed with Quikrete silica sand for comparison as a control. The commercially available Quikrete #1962 Medium sand is an Eglin silica sand (particle diameter 0.3–0.8 mm) quarried in Pensacola, Florida [16].

* Corresponding author.
E-mail address: hmarvi@asu.edu (H. Marvi).

https://doi.org/10.1016/j.powtec.2020.05.114
0032-5910/

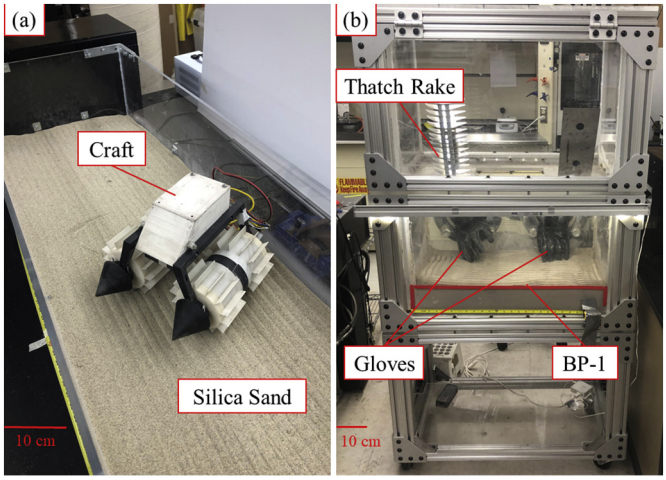

Fig. 1. (a) Craft with straight grousered wheels attached in silica sand bed and (b) simulant containment unit with tools displayed.

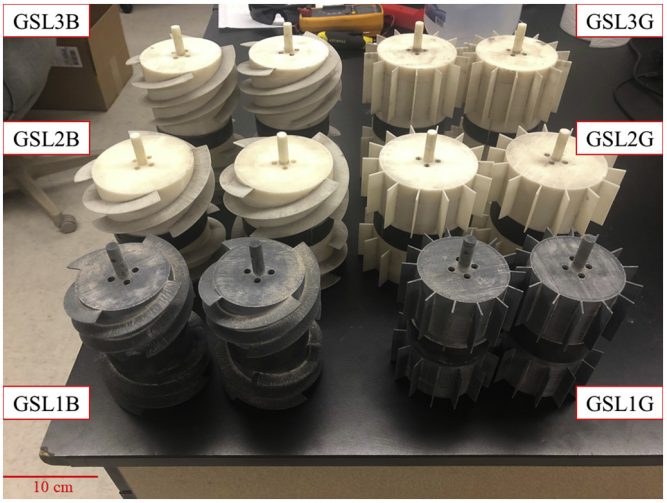

Fig. 2. The wheel sets used in experiments with helical grousers on the left and straight grousers on the right.

This class of sand is frequently used for granular locomotion experiments [17,18].

2. Evaluation of grousered wheels, a typical aspect of wheel design in granular media to avoid high slip. In this case, we evaluate both straight grousers and a new helical shape. While straight grousers obey the assumptions of the original laws, helical grousers do not, and neither has been evaluated by GSL.
3. Evaluation of a two motor wheeled craft with free vehicle dynamic movement.
4. Evaluation using three-dimensional MBD-DEM co-simulations at a target gravity. DEM simulations model individual particles and calculate collisions on a per-particle basis. MBD simulations model the dynamic reactions of linkages, including the kinematic chains of vehicles.
5. Evaluation of lighter rovers at faster speeds; the laws were originally evaluated at 2.33–4.76 RPM for 13.4–45.7 kg [15]. The set in this paper targets 13.1–75.0 RPM for approximately 1.5–3.0 kg.

The result is an investigation into the applicability of these laws when characteristics of the wheel-media interface are modified. This study also includes a direct performance characterization between helical grousers and straight grousers of the same blade thickness and length to gain insights into wheel design for different granular media.

2. Wheel design theory

The wheel shapes in this experiment are cylinders with two types of grousers as seen in Fig. 2. Grousers are protrusions added to the wheel rim to better engage the soil. This is done for the purposes of increasing the wheel's tractive ability. This may be considered similar to cleats on athletic shoes, although recent work [19] examining the subtle granular mechanism behind these apparent traction force gains shows a different cause (this is further discussed in section 2.1). The designations are "GSL" for the granular scaling law being evaluated, "1", "2", or "3" to distinguish different sets of parameters, described in Table 1, and "B" or "G" for bihelix and straight grouser shape, respectively. The sizing of the three sets is driven by GSL. The functional expression for GSL is presented in eq. 1 with parameters labelled on their physical counterparts in Fig. 3:

$$(P, V) = \psi(d, l, m, \omega, t, f, g, \rho, \mu, \mu_w) \tag{1}$$

On the left hand side of the equation are the target results of power P and translational velocity V. The right hand side is an uncharacterized function driven by the independent variables. The wheel is described by a characteristic length (radius or diameter) l, its depth into the page (wheel thickness) d, its mass m, and a driving rotational velocity ω. These physical characteristics are changed for the sizes of "1", "2", and "3". The wheel geometry is also defined by a consistent shape outline of points f. The wheel shape may be arbitrary (i.e smooth, grousers, lugs, etc) but may not change between a pair of scaled sets. This parameter is reflected by our two wheel shapes, the bihelix and straight grouser. One should not, for example, take the results from a smooth or straight grousered wheel and use it to predict results in a bihelix wheel. The environment is described by gravity g and the granular characteristics ρ, μ, and μ_w; these are density, internal friction, and wheel-grain friction, respectively. They are assumed constant and occur as a property of the granular environment and its interaction with the geometry. In our case, Quikrete and BP-1 will have different characteristics which illustrates why we can only predict the performance of a larger wheel from a smaller one in the same material. The system is also dependant on time, t, but during experimental trials for this paper the time-averaged outputs are discussed.

Using dimensional analysis, the function is transformed into a relationship between dimensionless parameters. To do this, the dimensions or base quantities of our system (length, mass, and time) are defined by the variables of function 1 as follows:

$$L = l \qquad M = m \qquad T = \frac{1}{\omega} = \sqrt{\frac{l}{g}} \tag{2}$$

Then, all parameters are transformed to dimensionless expressions using these equivalencies. For example, gravity has units of length over time squared; it can be reduced as follows:

Table 1
Properties of Straight Grousered and Bihelix Grousered Wheels.

Design	Diameter (cm)	Mass (kg)	Length (cm)	Blade Size (cm)	Target ω (RPM)
GSL1-G	7.50	1.459	14	1.250	15,30,45,60,75
GSL2-G	10.00	2.594	14	1.677	13,26,39,52,65
GSL3-G	9.375	2.918	18	1.563	14,27,40,54,67
GSL1-B	7.50	1.477	14	1.250	15,30,45,60,75
GSL2-B	10.00	2.626	14	1.677	13,26,39,52,65
GSL3-B	9.375	2.954	18	1.563	14,27,40,54,67

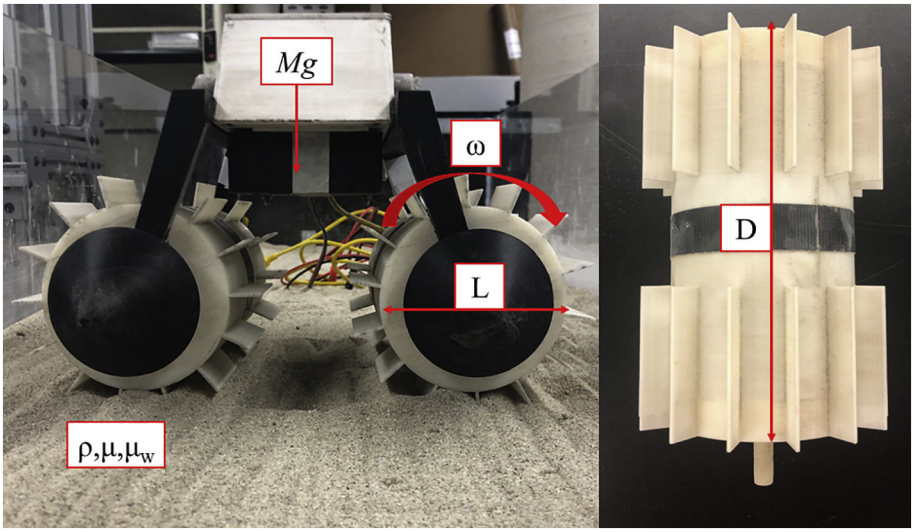

Fig. 3. Granular scaling parameters labelled for craft and straight grousered wheel.

$$\overline{g} = g_* \frac{T^2}{L} = \frac{g}{l\omega^2} \tag{3}$$

When this transformation is completed for all of the independent and dependant variables, the result can be expressed in the following two equivalent forms:

$$(\overline{P}, \overline{V}) = \Psi\left(\overline{d}, \overline{t}, f, \overline{g}, \overline{\rho}, \mu, \mu_w\right) \tag{4}$$

$$\left[\frac{P}{mg\sqrt{lg}}, \frac{V}{\sqrt{lg}}\right] = \Psi\left(\frac{d}{l}, t\sqrt{\frac{g}{l}}, f, \frac{g}{l\omega^2}, \frac{\rho l^3}{m}, \mu, \mu_w\right) \tag{5}$$

There are several items to note for the right hand sides of eqs. 4 and 5. The variables of l, m and ω were used to express the dimensions and their bar expressions would reduce to 1 i.e. $\frac{m}{m}$. This is why they are absent as bar expressions. The variables of f, μ, and μ_w were already dimensionless expressions; they did not change and are not different variables as the bar expressions are.

1. A set of assumptions and constraints simplifies eq. 5.
2. We assume constant gravity during experiments and between sets of wheels. This eliminates g from the equation, although this assumption will be relaxed during gravity-variant simulations in a later section.
3. We constrain the wheel thickness d and mass m to behave dependently, such that the ratio d/m is always constant. This constrains any change in d to act as if any n increase in thickness is identical to running n copies of the wheel. For example, if the thickness is doubled then the mass must also be doubled; this results in an identical pressure-sinkage relationship with the grains and would be the equivalent of running two of the originally sized wheels next to each other. To achieve this constraint, the expressions $\frac{d}{l}$ and $\frac{\rho l^3}{m}$ are no longer independent and instead expressed as their product.
4. We assume a homogeneous granular environment during experiments and between sets of wheels. Explicitly, this means that silica sand results can only be compared to other silica sand results. This implies a deep enough sinkage to eliminate any difference from surface effects between experiments as well. Finally, it eliminates ρ, μ, and μ_w from eq. 5 since the grains and their packing are assumed to remain the same.
5. The importance of consistency for wheel shape f has already been discussed, but this is now formally removed from the equation.
6. While power and velocity are a function of time, the results are concerned with comparing the steady state response of two wheels;

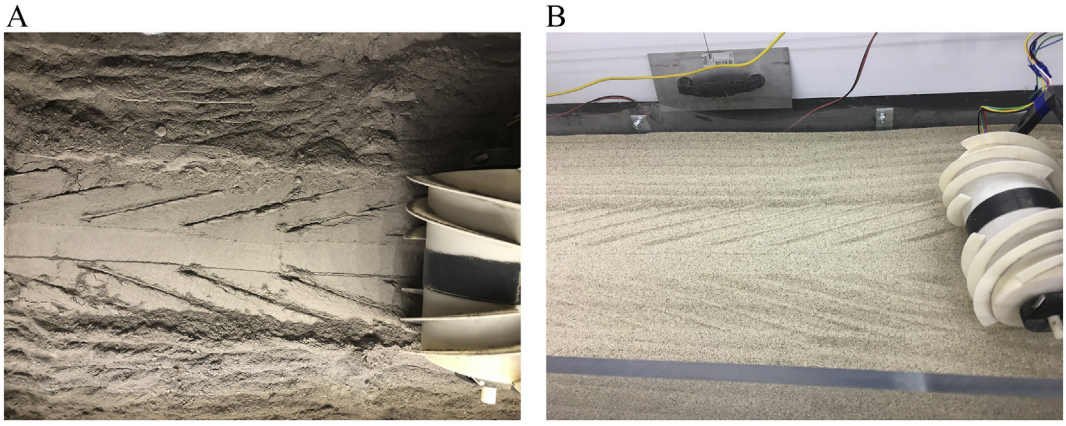

Fig. 4. Impression patterns left by helical grousers on both granular media (BP-1 on the left and Quikrete on the right).

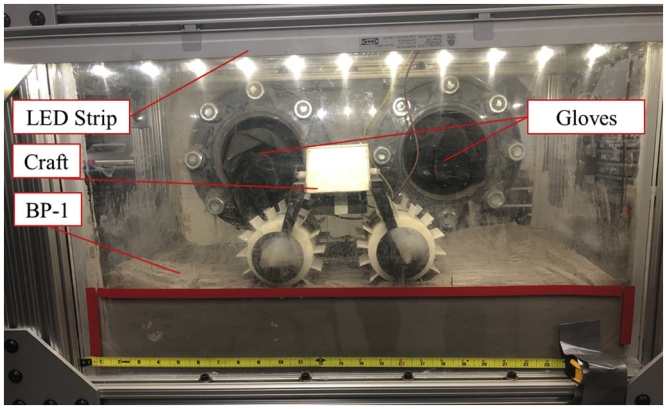

Fig. 5. BP-1 testing chamber with craft inside and components labelled.

removing the dependence on time, $\bar{t}$ is therefore eliminated from eqs. 4 and 5.

The above assumptions and constraints result in the following equation:

$$\left[\frac{P}{mg\sqrt{lg}}, \frac{V}{\sqrt{lg}}\right] = \tilde{\Psi}\left(\frac{1}{l\omega^2}, \frac{dl^2}{m}\right) \tag{6}$$

Observation shows that the correct dimensions have been balanced on either side of the equation and that four independent variables representing two expressions remain inside the dimensionless equation. If (l,m) are modified by scalars (r,s) with the new variables expressed as (l', m') and the two values in $\tilde{\Psi}$ are constrained to remain constant, then the following relationships are implied:

$$(l', m', d', \omega') = \left(rl, sm, \frac{s}{r^2}d, \frac{1}{\sqrt{r}}\omega\right) \tag{7}$$

$$P', V' = (s\sqrt{r}P, \sqrt{r}V) \tag{8}$$

If a wheel with the inputs of (l,m,d,ω) is subjected to experiments and the outputs (P,V) evaluated, then the outputs (P',V') from eq. 8 of a larger, heavier wheel are predictable assuming the relationships of eq. 7 are followed. This means that with two scalars, a mass scalar and a diameter scalar, plus a careful selection of complimentary input parameters, the power and velocity of a larger vehicle should be predictable from a smaller one. These scalars (r,s) are simply the ratios of diameter and mass between those two vehicles; putting these equations into practice will be seen in Table 1 of the next section.

2.1. Design of Straight Grousered Wheels

Grousers are a standard feature for vehicles and the shape of a straight grousered wheel adheres to the assumption of depth-invariant shape for the scaling laws. Yet research indicates that the motion gains or slip reduction of grousered wheels in soils are due to a "soil sweeping" effect rather than a thrust force increase from the grouser [19,20]. This effect causes a pre-clearing of granular material in front of the leading wheel edge before it makes contact. This lowers contact angle between wheel and soil wall and reduces the motion resistance effect of the media. We propose it is valuable to investigate GSL applied to a grousered wheel because while the outline adheres to the assumptions, this geometry-specific effect may prevent parameters from scaling properly. The minimum number of grousers necessary was determined by the following Eq. [21]:

$$\Phi < \frac{1}{1-i}\left(\sqrt{(1+h)^2-(1-z)^2} - \sqrt{1-(1-z)^2}\right), \tag{9}$$

where Φ is the spacing required between the grousers in radians, i is estimated slip, h is grouser height, and z is estimated sinkage, the depth below the granular surface which the wheel rim sinks to when engaged. To ensure the next grouser encounters soil before the wheel rim does, the placement of grousers around the wheel must be Φ radians or less. In our case, fourteen was the minimum required to clear material from the contact edge under 20% slip and approximately 2 cm of sinkage, our beginning estimates for the smaller sizes.

2.2. Design of Bihelix Grousered Wheels

There are few studies examining the mechanics of a helical or screw type grouser for wheeled traction. One study [22] indicated that a very wide angle with at least one grouser engaged at all times was most effective at generating drawbar pull force in a deformable tissue environment, but there were no studies about the granular mechanics interface with such a grouser. The granular physics behind why these wheels work deviates from that of traditional grousers. Straight grousers preclear material to avoid more resistive piles ahead of the round wheel shape. In contrast, helical grousers rely on the rigid-body coupling of the rotational motion of the helicoid shape with the forward translational motion of the wheel. As the wheel turns in granular media, the blade surface interfaces with the environment. From the frame of the material, the blades appear to translate along the axis of rotation. This results in an outward pushing force against the interlocked grains along the axis of rotation and perpendicular to the direction of travel. This force resists wheel slippage and contributes to the forward motion in the wheel, impacting the resultant slip. The outcome in the media is a continuous 2D projection of the 3D wheel, seen in Fig. 4.

Several design considerations went into the creation of the bihelix wheel. One was winding direction; all impacts being equal, we favored a helix shape which would tend to push material outwards, away from the wheel. We chose four helix windings, equally spaced around the wheel, to increase media engagement. The non-grousered space in the center was to avoid any interaction between helices or force concentrators where the blades would meet. All wheels, GSLG and GSLB, were printed on a Stratasys Mojo printer, with ABS, and assembled in halves and can be seen in Fig. 2.

As previously stated, a fundamental GSL assumption is uniformity of wheel shape along the axis of rotation. Explicitly, the arbitrary wheel shape outline is acceptable as long as it is uniform in this direction. A helical geometry will violate this and it is worth evaluating what level of deviation may be present. For a direct comparison of the grouser performance, the scaling of the wheel base was kept consistent between both wheel types; size is identical and mass differences are trivial between sets. The blade thickness and length of the helix are equal to the straight grouser thickness and length for each respective set. All target dimensions are listed in Table 1.

Using test parameters for both wheel shapes found in Table 1, the predicted power of the GSL2 sets should be approximately 205% (that is, double) of the GSL1 sets. The velocity should also be 115% of GSL1 velocity. For the GSL3 sets, the power should increase to 224% and velocity increase to 112%. If BP-1's properties lend themselves to scaling, we should see similar results in both granular media.

3. Methods to evaluate GSL performance

3.1. Development of BP-1 simulant containment unit

The lunar simulant used in this study was obtained from the Granular Mechanics and Regolith Operations Lab at NASA Kennedy Space Center (KSC), colloquially known as the "SwampWorks" Lab. The simulant,

Black Point 1 (BP-1), is made from the Black Point basalt flow in the San Francisco Volcanic Field. This is the lunar simulant NASA uses at KSC for testing the latest lunar robotics and in the robotic mining competition [23,24]. A full geotechnical assessment of BP-1 is available in the literature [16,25]. The important points we highlight for the purposes of our experiment are:

1. A D60 value of 0.11 mm, that is 60% of particle sizes are finer (smaller) than 110 μm
2. A classification of particle shape in the angular to sub-angular category
3. An internal angle of friction between 39 and 51°, somewhat dependant on bulk density

The result of the above properties is a granular media that, while only weakly cohesive, is pre-disposed to less flowability, more discrete deformation, sensitive to plastic deformation memory and high trenching [26] due to high particle interlock. For comparison, Quikrete medium used in experiments is a silica sand which is kilned, sieved, and washed. It is the original material used in the GSL literature and has particles primarily 0.3–0.8 mm in size. The mechanics of wheel-grain interface can vary significantly; preliminary Earth testing of Mars Curiosity Rover traversability showed the variability in wheel performance and interaction which can occur in different types of granular media [27]. Evaluating the performance of GSL in varied materials importantly examines which materials will obey this type of prediction and how they may deviate.

While BP-1 is generally harmless when undisturbed, it does present an occupational hazard when dusted in a confined space. Therefore, testing of lunar simulants are typically performed with some level of containment. A custom-made simulant containment unit is shown in Figs. 1 and 5. It is complete with sealed chemical glove holes for tool and craft manipulation, and deformable rubber sealing on the box lid to allow for power and control cables. A bar of LED lights helps with visual tracking conditions. The simulant bed has 37.5 cm × 67.5 cm interior dimensions. The box was created using commercially available acrylic and aluminum.

3.2. Design of concentrically embedded motor transmission

The craft was designed to be multi-purpose, allowing the wheels to be easily interchanged. A modular undercarriage weight holder was added to the bottom of the craft to adjust total mass for scaling. Craft height was adjusted to keep center of gravity as low as possible without interfering with the wheels. Furthermore, the wheel mount width was designed to prevent the granular flows from each wheel from actively interfering with each other during craft operation. The craft is pictured in Fig. 6 along with a Solidworks model of the internal concentric mechanisms. An internal motor drivetrain is optimal due to the dusty nature of the operational environment. Any external belt or chain drive system would be susceptible to dust accumulation. A 12 V DC motor is fastened to its housing, the motor sleeve, via two small screws. A wiretube with four radially symmetric pegs fits into a cutout pattern at the back end of the motor sleeve. The tube shape transitions to a hexagonal one, and this hexagonal tube is then locked to the feet of the craft to create a single rigid body. Shaft power is transmitted from the motor output shaft to the wheel hull through an aluminum set screw D-hub coupling. Thus, the power is transferred to the wheel body and the motor is held static by the rigid body of the wiretube mounts.

The unit relies on two bearings for rotation. The front bearing (not shown in Fig. 6) is pressure fit onto the front wheel shaft. These shafts can be seen on the wheels' tops in Fig. 2. The back bearing, a collar bearing, is affixed to the circular portion of the wiretube with a set screw. This collar bearing is pressure fit into an octagonal dust cover which seals the wheel cavity from BP-1 ingress. The dust cover also mates the bearing and wheel together and allows the wheel to spin around the static wiretube.

The main electronic components are comprised of an Arduino Uno R3, Pololu MC33926 dual motor driver, and one current sensor and wheel encoder per motor. The dual motor driver enabled the craft to adjust the voltage with response from an Arduino PID controller. In addition, Hall effect linear current sensors were implemented per motor immediately before input power. All electronics were enclosed and sealed in the craft body to minimize exposure to BP-1 dust.

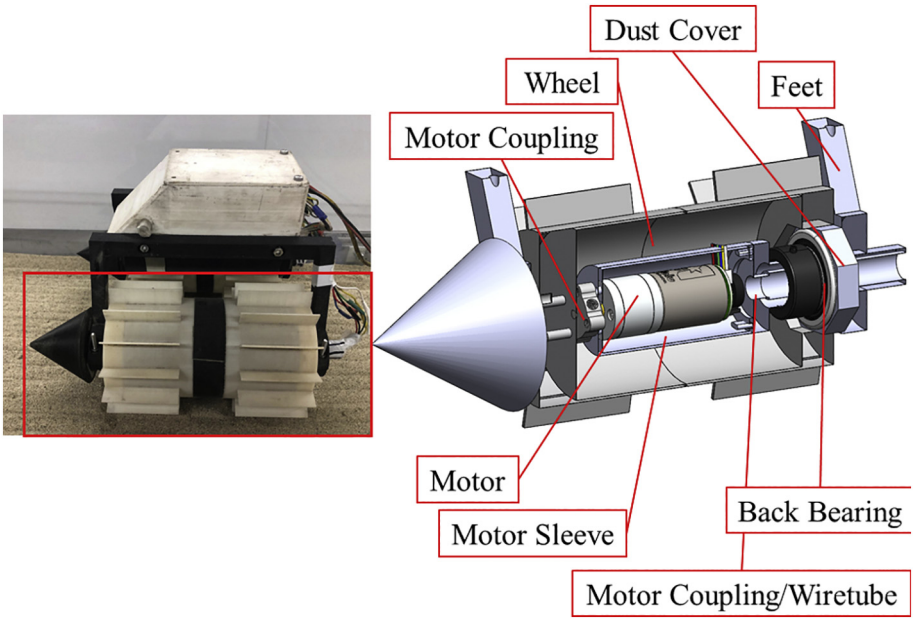

Fig. 6. Experimental craft with internal cutaway in Solidworks illustrating the power transfer mechanisms.

3.3. Experimental setup and procedure

Experiments were performed either in the simulant containment unit (BP-1) or a 80 cm × 250 cm sandbox (Quikrete). Experiments for either material began by tilling the soil with a handheld thatch rake to ensure no large soil stresses were present. Tilling was performed by the same team member for all 720 trials to ensure consistency. Craft was placed on top of either the BP-1 or Quikrete at one end of the respective test bed. The power supply was engaged and the craft completed a trial. The trial was recorded by both Arduino serial monitor for power and video camera for velocity. The simulant containment unit is equipped with a LED light strip so that the moving craft is clearly visible in the video as dusty conditions occur. Camera location and settings were kept consistent between all trials for each material. Blocks of color attached to all sides of the craft were used to enable its tracking. Utilizing the videos and a MATLAB based color tracking program, position versus time was determined and analyzed for each trial. The instantaneous velocity was calculated and used to evaluate steady state velocity per trial. Mechanical power was evaluated using in-line hall-effect current sensors to obtain individual current readings from each motor. Using the motor constant, current was converted to torque. The time-averaged torque and rotational speed were multiplied during steady state bands to produce time-averaged power. A total of 12 trials were performed for each set of speeds, five speeds were chosen for each wheel, and a total of six different wheel shapes were run in the two materials.

4. Results and discussion

4.1. Empirical performance of wheels in Quikrete and BP-1

Power draw data plotted in Fig. 7 indicate that the traditional grouser shape drew slightly less power than the bihelix grouser for all three sizes. This was true for both materials with the only notable exceptions being the two fastest speeds in BP-1 at the heaviest wheel size. It is worth bearing in mind that the bihelix design has not been optimized but still showed relatively similar trends to straight grousers in most BP-1 cases. Shape optimization, number of helices, grouser length, among other design factors are worth exploring, especially at a higher mass, slip, or sinkage. Chevron grousers have found success in low slip conditions [28] and are used on the Curiosity rover, and it would be a worthwhile future exercise to further investigate shape advantage. Straight grousers also resulted in higher velocity than bihelix wheels. Trends are seen in Fig. 8 with the GSLG sets generally shifted higher than GSLB regardless of size. This is displayed very plainly in the Quikrete experiments in addition to the "1" and "2" sizing in BP-1. However, the "3" sizing, the heaviest, shows a much narrower difference. This was also the set with nearly identical power draw for GSLG and GSLB.

4.2. Mechanical power ratio relationship to granular material, grouser shape, rotational speed, and motor placement

The central benefit behind GSL is the ability to predict large vehicle results from smaller ones. This can be expressed as a power or velocity ratio. For our study, the "2" and "3" size designations should result in power ratios of 2.05 and 2.24, respectively. Neither of these were fully reached; errors indicated that the larger crafts did not draw as much power as predicted. However, the ratios did show differentiation between experimental factors as seen in Fig. 9. For a set to be correctly predicted by GSL, all data ought to fall on the black line.

Higher error is present in the lunar simulant than Quikrete for all four shapes. Errors for all but the lowest speeds were 29–35%, 19–27%, 30–36%, and 13–17% for 2B, 3B, 2G, and 3G. Error for the slowest speeds of each set were 52%, 44%, 33%, and 30%, respectively. Conversely, the silica sand remained relatively consistent in level of error across sets. It also saw a much lower error in general. Errors for all speeds were 9–29%, 5–24%, 16–25%, and 16–24% for 2B, 3B, 2G, and 3G, respectively. Both the "2" and "3" sizes appear to have similar trend in moving further away from the line with higher power draw, and indeed the furthest points are the fastest speeds in BP-1 for both sizes. However, it is apparent that the heavier of the two sets, "3", resulted in lower error for both shapes in BP-1. We will also note that the data for GSL2G and GSL3G in Quikrete, the material used in original GSL testing, were remarkably consistent in power ratio error. While we saw prediction errors of 15–25% across speeds, their values at each speed held a difference of less than 1% except for the slowest speed, meaning the error of GSL2G and GSL3G for comparable speeds was near identical.

After examining the comparisons, one concludes that the shape of the grouser made little difference in this set of experiments, that the larger mass difference in the "3" case made them marginally more accurate, that the data deviated from the prediction line with increased speed, and in general, that BP-1 showed more error than Quikrete. However, this means that despite the error, the bihelix shape generally conformed to the scaling laws as well as straight grousers and BP-1 was only marginally worse than Quikrete in predictive results.

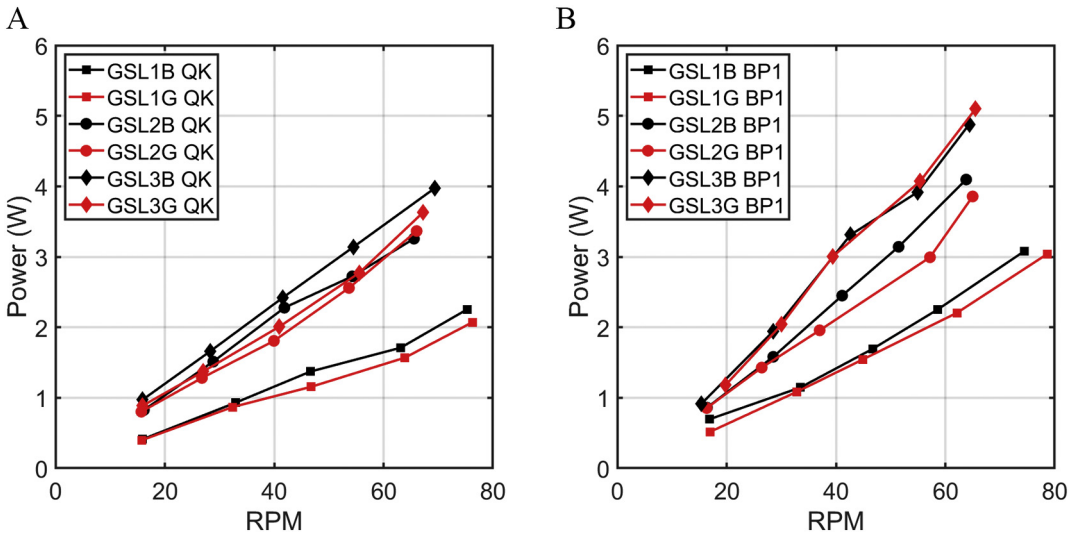

Fig. 7. Comparison of craft power draw in the two materials, Quikrete on left and BP-1 on right.

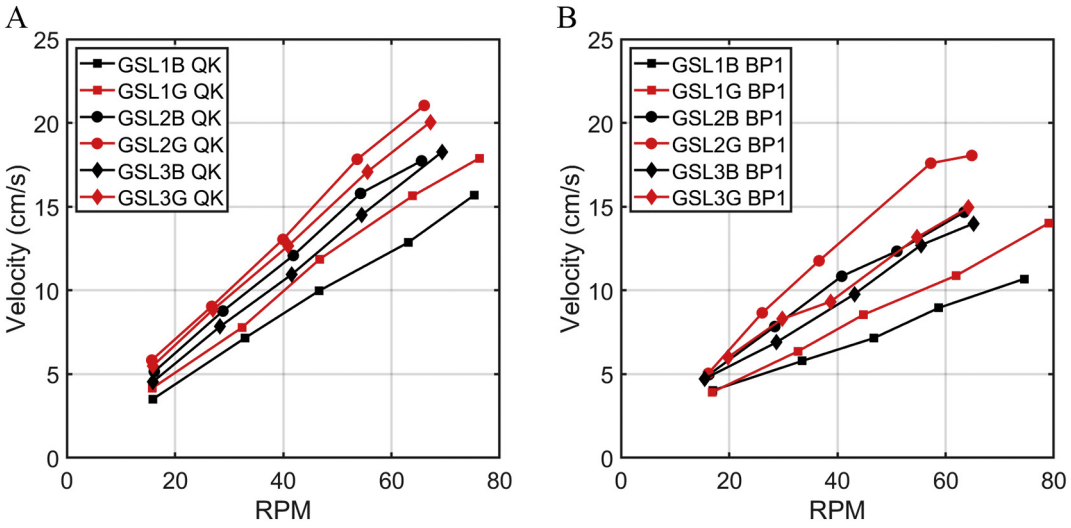

Fig. 8. Comparison of craft velocity in the two materials, Quikrete on the left and BP-1 on the right.

Differentiating the velocity ratio prediction by material yields a much starker contrast than the power predictions (Fig. 10). In BP-1, the error for 2G, 3G, 2B, and 3B was 17–27%, 3–15%., 7–24%, and 0–21%, respectively. In all cases, the larger and heavier craft moved faster than predicted and this trend generally increased with wheel speed. For the Quikrete, results were much closer in both accuracy and precision. The GSL2G set contained error in the 0.6% to 6.8% range, the GSL3G in 0.8–9.1%, GSL2B in 0.1–3.8% for all but the lowest speed (17%), and GSL3B in 0.1–4.9% across the entire set.

The translational velocity error was significantly lower than power error partially because velocity was the driving variable; we set the target rotation and drew the necessary power to achieve it. Assuming relatively consistent slip conditions, the velocity would be very close. We see consistent velocity prediction with the largest differentiator being material, and a slightly more accurate prediction with straight grousers in BP-1 than the helices.

4.3. Discussion of errors

If we examine the range of the three fastest speeds for Quikrete in this study, all comparisons have errors below 4%. This close agreement to velocity predictions occurs despite a rotational velocity range more than an order of magnitude larger than the originally reported results [15] performed at 2.33–4.76 RPM. However, there is a similar decrease of nearly an order of magnitude in mass in this study from the 13.4–45.7 kg of the originally reported results. What we can infer is that when interacting with Quikrete silica sand and similar flowable media, the granular mechanics support good estimated predictions of velocity using GSL at these particular combinations of speeds and masses. However, it remains to be seen what level of increase in inertial forces produces noticeable deviations. As previously mentioned, the BP-1 velocity error was wholly underpredicted from the results of the GSL1 sizing. The larger and heavier craft moved faster than it ought to for all cases and this error only increased with speed. While there are no comparative experiments to point to, the most likely explanation is the high interlock of the media and lack of flowability. If the particles interlocked and compressed into a less deformable surface with increased mass, it would explain why it drew less power and rotated faster than predicted.

Additional context for both of these can be found as we turn to the power error. Recent investigations specifically examine how the mass or velocity may affect the scaling laws [29]. The work examined how these parameters affected power draw, and found a stronger correlation with mass. As mass for a set increased (while keeping the scalar of the pair the same), the error decreased and power draw was closer to

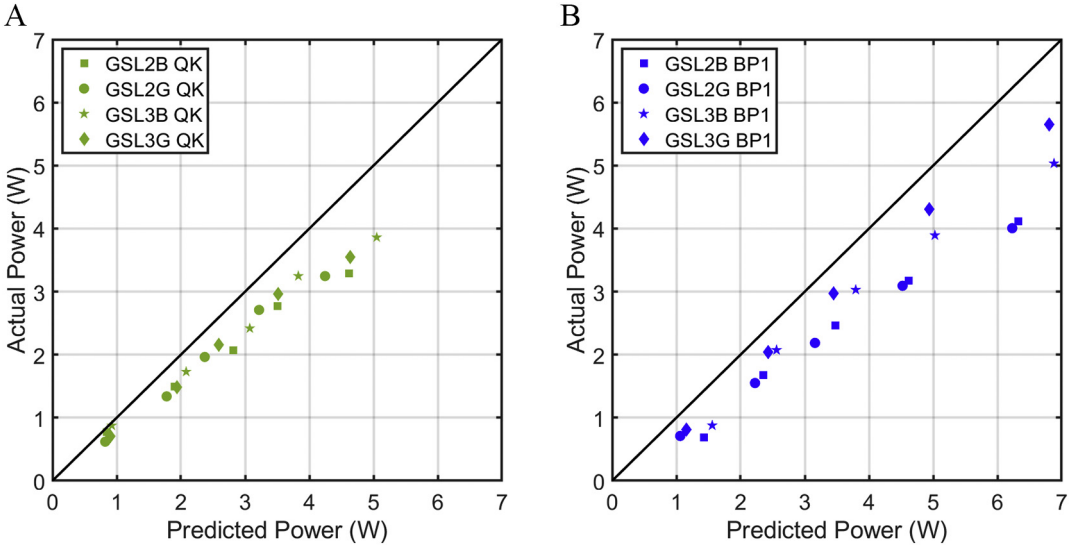

Fig. 9. Predicted power versus measured power consumption with black line indicating perfect prediction. Quikrete on the left and BP-1 on the right.

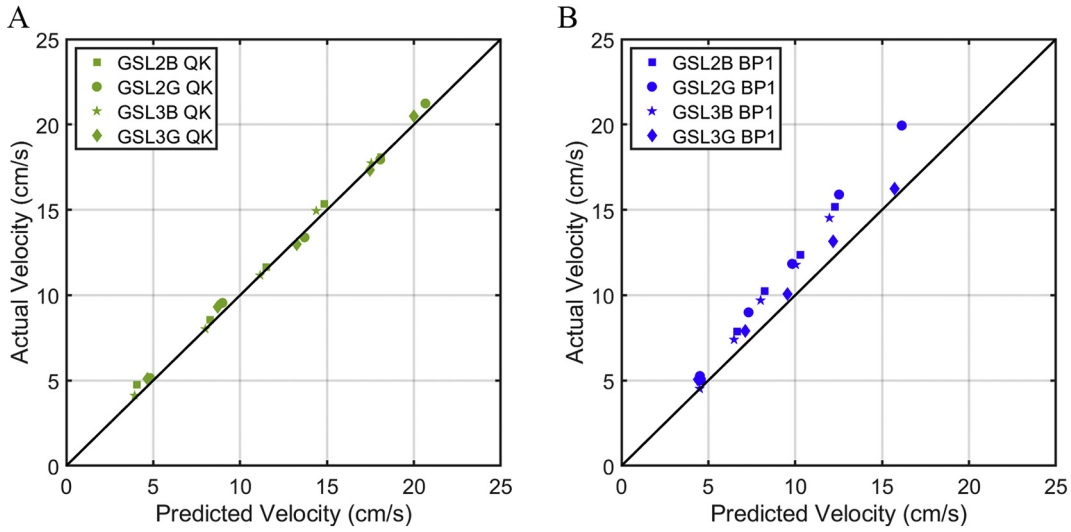

Fig. 10. Predicted velocity versus measured velocity with black line indicating perfect prediction. Quikrete on the left and BP-1 on the right.

prediction. However, there is a notable error increase with increased rotational velocity for the heavier sets. The faster these heavy sets go, the lower the power draw is compared to prediction. This supports the hypothesis of inertial forces contributing some level of error.

An interesting point of note is that linear regression of the power error as a function of craft mass for all speeds was very similar for both the current study and the previous study. We previously predicted a total elimination of error for grousered wheels in silica sand at approximately 8 kg [29] and calculations from this work predict it at 9 kg. This led to the current hypothesis for large power error levels: shallow sinkage. The assumption of a continuous body of grains subject to frictional plasticity requires the internal friction coefficient remain constant [14] and the grains behave as a single block. If sinkage is insufficient and a non-trivial portion of the experiment occurs at surface level, then there is an increased likelihood that surface effects will introduce inconsistencies in the predictions.

Pulling from this previous work, craft with grousered wheels identical in size and mass to GSL2G in this study exhibited similar power errors. Additional investigation of experimental preparation and results showed that trials of these wheels in raked preparation sand only obtained 2.02 ± 0.19 mm of sinkage. The average difference in peak/valley of the raking for all 40 trials was 1.58 ± 0.18 mm. In sand which was unraked and smoothed, sinkage for these GSL2G wheels was 0.69 ± 0.12 mm. The particle size of Quikrete sand is generally between 300 and 800 μm and a depth of ten grain diameters would be between 3 and 8 mm. Sinkage was never observed to exceed 3 mm on average for those previous tests and it is unlikely it was achieved in this study as well, especially since scaling between wheel shapes is similar. Thus, we can draw a similar conclusion about the Quikrete error in this study: shallow sinkage in general, and at a similar magnitude to sand preparation patterns, led to a difference in grain packing and/or grain size surface effects violating frictional plasticity which altered the effective friction of the environment.

For BP-1, current hypothesis is that shallow sinkage is partly the cause of power prediction error as well. However, this does not explain the greater inconsistency of error. The root of this may be driven by different granular mechanics for the BP-1 particles. We turn to the Mohr-Coulomb criterion:

$$\tau = c + \sigma \tan\phi \tag{10}$$

Where τ is shear stress, c is cohesion, σ is normal pressure and ϕ is angle of internal friction. As noted in the geotechnical evaluation [25], the friction angle of BP-1 is highly variant with bulk density, ranging from 39 to 51 deg. This varies the coefficient for the normal pressure in the shear stress equation between 0.81 and 1.235. Error variation might occur with bulk density differences between sets of trials and this would violate one of the assumptions (constant density). While we cannot say quantitatively exactly what the stress variation was, we can say qualitatively that it would likely be of significant magnitude. The conclusion for power error difference is then that both materials violated necessary sinkage assumptions, but BP-1 did so at inconsistent levels.

Similarly, we also remark that the tractive ability of a craft is directly related to the amount of shear stress that the soil can bear. Given that both the cohesion and the entire range of possible friction angles are higher in BP-1 than in Quikrete, it is likely that the threshold for the media to flow in an acceptably consistent manner is higher as well. That is, the greater shear strength of BP-1 possibly amplified the power errors by providing more support than predicted for heavier sets due to surface effects. Similarly, while Quikrete did not sink deep enough to scale power properly, it flowed relatively well and in a predictable manner for velocity scaling. The BP-1, possessing a higher shear strength, allowed greater traction for the wheels than scaling predicted and amplified surface effects. This would explain the relatively more accurate Quikrete velocity predictions and the much higher velocity than predicted in the larger sets tested in BP-1.

4.4. MBD-DEM simulations for gravity-variant GSL

Environments where scaling predictions hold significant application include bodies of different gravity. The closest and most visited target is that of Earth's moon. The gravity is roughly 1/6 of Earth's, a suitable order of magnitude for evaluating these laws. Results of studies comparing reduced weight rovers in earth granular media experiments versus identical experiments performed on parabolic flights with direct gravity variation have shown significant differences [5,30]. In some cases, the trends are actually inverted; granular compaction due to gravity plays a significant role in granular physics for rover motion. It is therefore of great interest whether tests at Earth gravity could be theoretically extrapolated to predict performance in lower gravity environments. For this, we will create a simulated environment with both multi-body dynamics (MBD) of the craft and discrete element method (DEM) for the media as seen in Fig. 11. DEM simulations model individual particles and calculate collisions on a per-particle basis. Modeling the granular deformation under vehicles has been done before [31] and testing deformable materials [32–37], evaluating additive manufacturing [38,39], analyzing jamming/packing problems [40,41] and modeling

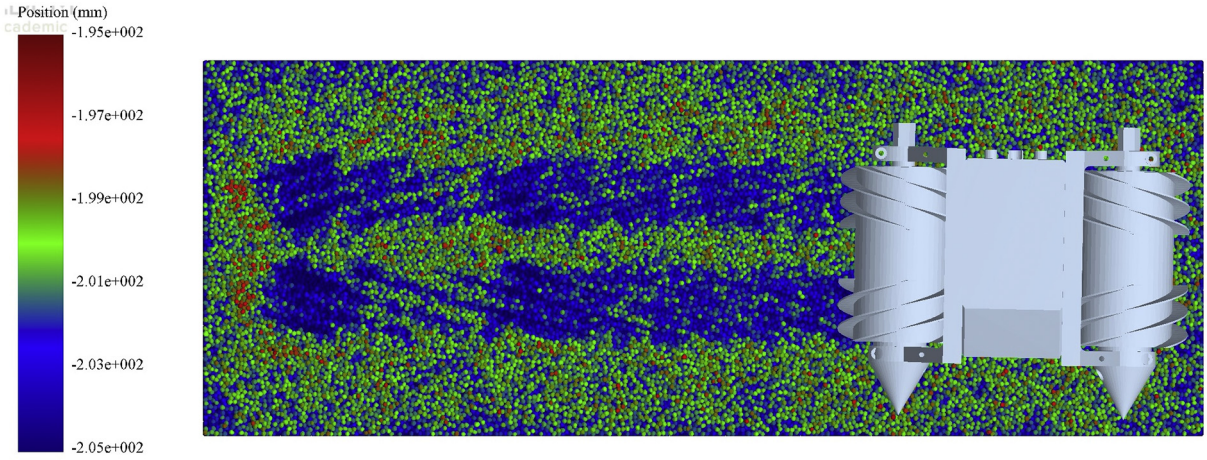

Fig. 11. Top view of an MBD-DEM simulation with particles color coded by depth.

particle beds [42,43] are a few of the other applications. DEM can be combined with other numerical methods such as finite element modeling (FEM) [44–46] including for vehicles [47,48] and in this study is combined with MBD. MBD models the dynamic linkages of the vehicle itself and their reactions. It can provide additional insights to experimental systems which may be otherwise difficult to obtain [49–52]. MBD-DEM has been used for mobility including reduced gravity simulations looking at wheel-terrain interfaces [53,54] and comparing Earth and lunar gravity for scaling in this manner has seen previous success [55].

Recall the earlier scaling eq. 6 for power and velocity. We now address the conclusion of the gravity-variant version. If a wheel with the inputs of (g,L,M,D,ω) is compared to a wheel affected by positive scalars r, s, and q (for gravity) the predicted relationship $(g',L',M',D',\omega') = (qg,rL,sM,sr^{-2}D,q^{1/2}r^{-1/2}\omega)$ follows. The conclusion is that one should be able to predict the time-averaged power and translational velocity of a rotating wheel even in a different gravity with the following relationship:

$$P' = q^{3/2}r^{1/2}sP \tag{11}$$

$$V' = (qr)^{1/2}V \tag{12}$$

Due to the computationally demanding nature of these simulations, we selected only one wheel, the GSLB set, to perform in as close a match to the lunar soil as possible. We have listed the properties entered into the DEM simulation in Table 2, and we note here that the results seen are not directly comparable to BP-1. However, the properties of this artificial granular material match that of BP-1 or basalt as best found in the literature. Since there is little literature about the friction interactions of plastics with rocks and the surface properties of printed plastics can vary, these parameters were evaluated experimentally. A plate was sprayed with adhesive and dusted with BP-1 to form a flat surface, and 3 mm stainless steel spheres were dusted as well. The rolling and static friction of BP-1 on ABS and BP-1 on BP-1 were then determined experimentally using modified tilt tests and ASTM G194 and ASTM G219 tests. The average from 20 tests was then used as the value for each. Particle size and Young's modulus were the only properties intentionally altered; these were changed since they play a direct role in computation time. The particles in the simulation are all multi-sphere shapes; the granular environment is comprised of 50% bisphere clumps and 50% tetrasphere clumps. GSL1B is run in a simulated BP-1 environment in Earth gravity. GSL2B/3B are run in an identical environment with lunar gravity and adequate time for particle settling. Power and velocity are compared to their predictions in Fig. 2. To our knowledge, this is the first evaluation of GSL for a fully three-dimensional MBD-DEM two-wheeled vehicle simulated in a target gravity and environment.

The results seen in Fig. 12 indicate a close match with the gravity-variant scaling laws for both power and velocity ratios. In the GSL2B scaling power prediction, every datapoint but that of fastest speed showed 5–8% error. In the GSL3B scaling power prediction, every speed but the fastest showed 1–5% error. The fastest speeds had 19% and 12% error in GSL2B and 3B, respectively. In all but the slowest cases, the error was positive; that is, the craft drew more power than predicted during the lunar gravity cases. The majority of velocity scaling predictions were at less than 2% error; GSL2B error was below 2% for all but slowest speed (5%) and GSL3B ranged from 0.2%–3.3%. We note that the simulation environment is able to provide a much more ideal preparation of material which likely created adequate conditions for GSL to make successful predictions. We also show that the gravity-variant scaling laws can successfully predict power and velocity for a larger vehicle in lunar gravity from a smaller vehicle in Earth gravity, in a simulated three-dimensional environment of granular media. While this is promising, the errors for lightweight craft in the BP-1 lunar analogue indicate that future work will be necessary before this can be experimentally applied.

5. Conclusions and future work

The data presented supports important criteria of feasibility for using GSL. Using a lightweight, two-wheeled, unrestrained craft with two grouser designs we see significant deviations in craft power from predictions in silica sand and crushed basalt. In particular, we note the root cause of these power prediction deviations to be shallow sinkage which leads to a violation of assumed constant friction coefficient in the environment from surface effects. We highlight the importance of a sinkage criterion of 10× average particle size as a first order evaluation

Table 2
Properties of simulated materials and interactions.

Material Property	BP-1	ABS
Poisson's Ratio	0.25	0.35
Density (kg/m^3)	3150	1070
Young's Modulus (Pa)	73E7	1.8E9
Interactive Property	**BP1-BP1**	**BP1-ABS**
Coefficient of Restitution	0.8	0.8
Coefficient of Static Friction	0.56	0.57
Coefficient of Rolling Friction	0.07	0.17
Other Properties	**Value**	
Size of Bisphere clump	3 mm	
Size of Tetrasphere clump	3.75 mm	
Simulation Timestep	9.6E-6 s	

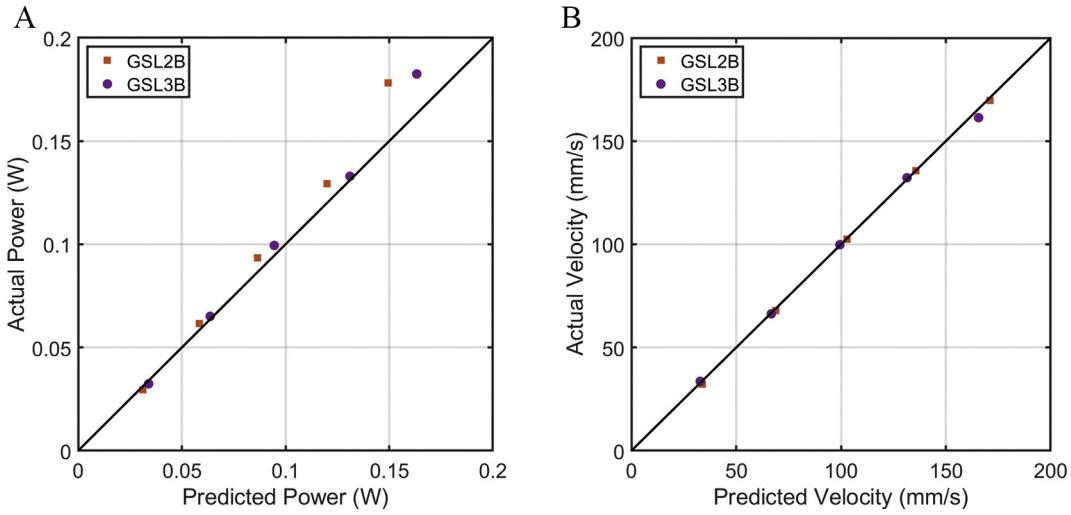

Fig. 12. Simulation results paired with their respective predictions with solid black line indicating perfect prediction.

for future studies. We also see significant deviations in velocity predictions in crushed basalt but not silica sand. We note this lack of observed error indicates that shallow sinkage alone does not create these errors. We hypothesize that the crushed basalt's small particle size combined with high interlock led to increased tractive performance and explains underprediction of velocity for all wheel types in BP-1. Finally, MBD-DEM simulations show a promising avenue of evaluating gravity-variant rover prediction with GSL.

There are several proposed future avenues to expand this work. Additional work with media similar to BP-1 can examine whether this material will obey a granular scaling law for wheels or other shapes. The sinkage threshold for each individual material should be confirmed before using GSL in vehicle design. Exploring other dimensionless terms of interest, other dependent variables, could be of use. Power and velocity were chosen as the outputs, but other outputs could be selected and derived. An example is drawbar pull, the total tractive force generated from a wheel's interaction with the granular environment. This is also expressed as a difference between the thrust generated and the motion resistance of the terrain against the wheels. Drawbar pull is often used as a performance characteristic for vehicle engineers and was proposed as a future avenue in the original GSL paper [15].

The mass scalar in a similar study [29] was 1.778 for all sets. In this study, 1.778 and 2.0 are used. In the Slonaker et al. study, mass scalars were 2.18–2.40. While this difference in scalars is not trivial, it is not immediately obvious how it may influence error. The scalars of 1.778 and 2.0 were chosen as similar ratios to the Slonaker et al study which could be successfully implemented experimentally in the BP-1 chamber but this range could be expanded in other experiments. For example, we see that the Slonaker et al. study confirmed that a wheeled experiment can be used to predict performance of a wheel of twice the mass in silica sand. However, it would be good to know if there is an upper bound or any other limits to the implementation. This is another parameter to examine as well. Further examination of error as a function of wheel velocity could also determine how to apply these laws in practice for vehicles which move faster than those in laboratory environments. Finally all of these ought to be done with the mass and speed of the craft in mind and simple benchmark sinkage tests ought to be performed to determine if the experiment meets GSL criteria.

Declaration of Competing Interest

The authors declare that they have no known competing financial interests or personal relationships that could have appeared to influence the work reported in this paper.

Acknowledgements

The authors would like to thank members of the BIRTH Lab for their assistance and Arizona State University for the funding.

References

[1] M.G. Bekker, Theory of Land Locomotion, University of Michigan Press, 1956.
[2] M.G. Bekker, Introduction to Terrain-Vehicle Systems. Part I: The Terrain. Part II: The Vehicle, Technical Report Michigan Univ Ann Arbor, 1969.
[3] M.G. Bekker, Mechanics of locomotion and lunar surface vehicle concepts, SAE Trans. (1964) 549–569.
[4] J.Y. Wong, Theory of Ground Vehicles, John Wiley & Sons, 2008.
[5] J. Wong, Predicting the performances of rigid rover wheels on extraterrestrial surfaces based on test results obtained on earth, J. Terrramech. 49 (2012) 49–61.
[6] F.J. Comin, W.A. Lewinger, C.M. Saaj, M.C. Matthews, Trafficability assessment of deformable terrain through hybrid wheel-leg sinkage detection, Journal of Field Robotics 34 (2017) 451–476.
[7] A. Gallina, R. Krenn, M. Scharringhausen, T. Uhl, B. Schäfer, Parameter identification of a planetary rover wheel–soil contact model via a bayesian approach, Journal of Field Robotics 31 (2014) 161–175.
[8] J. Aguilar, T. Zhang, F. Qian, M. Kingsbury, B. McInroe, N. Mazouchova, C. Li, R. Maladen, C. Gong, M. Travers, et al., A review on locomotion robophysics: the study of movement at the intersection of robotics, soft matter and dynamical systems, Rep. Prog. Phys. 79 (2016), 110001.
[9] R.D. Maladen, Y. Ding, C. Li, D.I. Goldman, Undulatory swimming in sand: subsurface locomotion of the sandfish lizard, science 325 (2009) 314–318.
[10] Y. Ding, N. Gravish, D.I. Goldman, Drag induced lift in granular media, Phys. Rev. Lett. 106 (2011), 028001.
[11] C. Li, T. Zhang, D.I. Goldman, A terradynamics of legged locomotion on granular media, science 339 (2013) 1408–1412.
[12] T. Zhang, D.I. Goldman, The effectiveness of resistive force theory in granular locomotion, Phys. Fluids 26 (2014), 101308.
[13] A. Thoesen, S. Ramirez, H. Marvi, Screw-generated forces in granular media: experimental, computational, and analytical comparison, AIChE J. 65 (2019) 894–903.
[14] H. Askari, K. Kamrin, Intrusion rheology in grains and other flowable materials, Nat. Mater. 15 (2016) 1274.
[15] J. Slonaker, D.C. Motley, Q. Zhang, S. Townsend, C. Senatore, K. Iagnemma, K. Kamrin, General scaling relations for locomotion in granular media, Phys. Rev. E 95 (2017), 052901.
[16] V. Nardelli, M. Coop, J. Andrade, F. Paccagnella, An experimental investigation of the micromechanics of eglin sand, Powder Technol. 312 (2017) 166–174.
[17] J.Y. Wong, C. Senatore, P. Jayakumar, K. Iagnemma, Predicting mobility performance of a small, lightweight track system using the computer-aided method ntvpm, J. Terrramech. 61 (2015) 23–32.
[18] S. Agarwal, C. Senatore, T. Zhang, M. Kingsbury, K. Iagnemma, D.I. Goldman, K. Kamrin, Modeling of the interaction of rigid wheels with dry granular media, J. Terrramech. 85 (2019) 1–14.
[19] S.J. Moreland, Traction Processes of Wheels on Loose, Granular Soil, Ph.D. thesis, Doctoral Dissertation Carnegie Mellon University, 2013.
[20] S. Moreland, K. Skonieczny, H. Inotsume, D. Wettergreen, Soil behavior of wheels with grousers for planetary rovers, IEEE Aerospace Conference, IEEE 2012, pp. 1–8.
[21] K. Skonieczny, S.J. Moreland, D.S. Wettergreen, A grouser spacing equation for determining appropriate geometry of planetary rover wheels, IEEE/RSJ International Conference on Intelligent Robots and Systems, IEEE 2012, pp. 5065–5070.
[22] M.E. Rentschler, S.M. Farritor, K.D. Iagnemma, Mechanical design of robotic in vivo wheeled mobility, J. Mech. Des. 129 (2007) 1037–1045.

[23] R.P. Mueller, Lunabotics mining competition: Inspiration through accomplishment, Earth and Space 2012: Engineering, Science, Construction, and Operations in Challenging Environments 2012, pp. 1478–1497.
[24] R.P. Mueller, P.J. Van Susante, A review of extra-terrestrial mining robot concepts, Earth and Space 2012: Engineering, Science, Construction, and Operations in Challenging Environments 2012, pp. 295–314.
[25] E. Suescun-Florez, S. Roslyakov, M. Iskander, M. Baamer, Geotechnical properties of bp-1 lunar regolith simulant, J. Aerosp. Eng. 28 (2014), 04014124.
[26] I. Townsend, A.C. Muscatello, D. Dickson, L. Sibille, A. Nick, K. Leucht, G. Tamasy, Mars isru pathfinder regolith autonomous operations-modeling and systems integration, AIAA SPACE and Astronautics Forum and Exposition 2020, p. 5150.
[27] M. Heverly, J. Matthews, J. Lin, D. Fuller, M. Maimone, J. Biesiadecki, J. Leichty, Traverse performance characterization for the mars science laboratory rover, Journal of Field Robotics 30 (2013) 835–846.
[28] H. Inotsume, K. Skonieczny, D.S. Wettergreen, Analysis of grouser performance to develop guidelines for design for planetary rovers, Proceedings of the 12th International Symposium on Artificial Intelligence, Robotics and Automation in Space (I-SAIRAS 2014), 2020.
[29] A. Thoesen, T. McBryan, M. Green, J. Martia, D. Mick, H. Marvi, Revisiting scaling laws for robotic mobility in granular media, IEEE Robotics and Automation Letters 2 (2) (2020) 1319–1325.
[30] T. Kobayashi, Y. Fujiwara, J. Yamakawa, N. Yasufuku, K. Omine, Mobility performance of a rigid wheel in low gravity environments, J. Terrramech. 47 (2010) 261–274.
[31] J.B. Johnson, P.X. Duvoy, A.V. Kulchitsky, C. Creager, J. Moore, Analysis of mars exploration rover wheel mobility processes and the limitations of classical terramechanics models using discrete element method simulations, J. Terrramech. 73 (2017) 61–71.
[32] T. Leblicq, S. Vanmaercke, H. Ramon, W. Saeys, Discrete element modelling of bendable tubes, Int. J. Mech. Sci. 94 (2015) 75–83.
[33] P.M. Pieczywek, A. Zdunek, Compression simulations of plant tissue in 3d using a mass-spring system approach and discrete element method, Soft Matter 13 (2017) 7318–7331.
[34] Y. Guo, C. Wassgren, W. Ketterhagen, B. Hancock, J. Curtis, Discrete element simulation studies of angles of repose and shear flow of wet, flexible fibers, Soft Matter 14 (2018) 2923–2937.
[35] R. Gibaud, E. Guesnet, P. Lhuissier, L. Salvo, Modeling large viscoplastic strain in multi-material with the discrete element method, Int. J. Mech. Sci. 136 (2018) 349–359.
[36] X. Li, W. Li, S. Yang, Z. Hao, H. Shi, Study on polyurethane media for mass finishing process: dynamic characteristics and performance, Int. J. Mech. Sci. 138 (2018) 250–261.
[37] Y. Xu, F. Dai, H. Du, Experimental and numerical studies on compression-shear behaviors of brittle rocks subjected to combined static-dynamic loading, Int. J. Mech. Sci. 175 (2020), 105520.
[38] E.J. Parteli, T. Pöschel, Particle-based simulation of powder application in additive manufacturing, Powder Technol. 288 (2016) 96–102.
[39] H. Xin, W. Sun, J. Fish, Discrete element simulations of powder-bed sintering-based additive manufacturing, Int. J. Mech. Sci. 149 (2018) 373–392.
[40] W. Liu, S. Li, A. Baule, H.A. Makse, Adhesive loose packings of small dry particles, Soft Matter 11 (2015) 6492–6498.
[41] M.Z. Miskin, H.M. Jaeger, Evolving design rules for the inverse granular packing problem, Soft Matter 10 (2014) 3708–3715.
[42] R. Yoshimatsu, N.A. Araújo, T. Shinbrot, H.J. Herrmann, Field driven charging dynamics of a fluidized granular bed, Soft Matter 12 (2016) 6261–6267.
[43] J. Chen, O. Orozovic, K. Williams, J. Meng, C. Li, A coupled dem-sph model for moisture migration in unsaturated granular material under oscillation, Int. J. Mech. Sci. 169 (2020), 105313.
[44] O. Kudryavtsev, S. Sapozhnikov, Numerical simulations of ceramic target subjected to ballistic impact using combined dem/fem approach, Int. J. Mech. Sci. 114 (2016) 60–70.
[45] B. Harthong, J.-F. Jérier, V. Richefeu, B. Chareyre, P. Dorémus, D. Imbault, F.-V. Donzé, Contact impingement in packings of elastic–plastic spheres, application to powder compaction, Int. J. Mech. Sci. 61 (2012) 32–43.
[46] Z. Zheng, M. Zang, S. Chen, C. Zhao, An improved 3d dem-fem contact detection algorithm for the interaction simulations between particles and structures, Powder Technol. 305 (2017) 308–322.
[47] P. Yang, M. Zang, H. Zeng, An efficient 3d dem-fem contact detection algorithm for tire-sand interaction, Powder Technol. 360 (2020) 1102–1116.
[48] H. Zeng, W. Xu, M. Zang, P. Yang, Calibration of dem-fem model parameters for traction performance analysis of an off-road tire on gravel terrain, Powder Technol. 362 (2020) 350–361.
[49] D.K.A. Patel, B.P. Patel, M.K.A. Pate, A critical review on kinematics of hydraulic excavator backhoe attachment, International Journal of Mechanical Engineering and Robotics Research 4 (2015) 188.
[50] M.K. Al-Solihat, M. Nahon, Flexible multibody dynamic modeling of a floating wind turbine, Int. J. Mech. Sci. 142 (2018) 518–529.
[51] D.L. Schott, S.W. Lommen, R. van Gils, J. de Lange, M.M. Kerklaan, O.M. Dessing, W. Vreugdenhil, G. Lodewijks, Scaling of particles and equipment by experiments of an excavation motion, Powder Technol. 278 (2015) 26–34.
[52] S. Lommen, M. Mohajeri, G. Lodewijks, D. Schott, Dem particle upscaling for large-scale bulk handling equipment and material interaction, Powder Technol. 352 (2019) 273–282.
[53] T.M. Wasfy, D. Mechergui, P. Jayakumar, Understanding the effects of a discrete element soil model's parameters on ground vehicle mobility, J. Comput. Nonlinear Dyn. 14 (2019).
[54] A. Recuero, R. Serban, B. Peterson, H. Sugiyama, P. Jayakumar, D. Negrut, A high-fidelity approach for vehicle mobility simulation: nonlinear finite element tires operating on granular material, J. Terrramech. 72 (2017) 39–54.
[55] A. Thoesen, T. McBryan, H. Marvi, Helically-driven granular mobility and gravity-variant scaling relations, RSC Adv. 9 (2019) 12572–12579.